Sources of Transconductance Collapse in III–V Nitrides—Consequences of Velocity-Field Relations and Source/Gate Design

Yuh-Renn Wu, *Student Member, IEEE*, Madhusudan Singh, *Student Member, IEEE*, and Jasprit Singh

***Abstract*—Experimental results from submicrometer devices in III–V nitride devices often exhibit a significant decrease in the transconductance when gate bias is increased. This creates new challenges for circuit design in III–V nitride technology. In this paper, we discuss possible sources of this collapse from a theoretical and computational standpoint. We find that polar optical phonon emission related velocity-field nonlinearities in 5–40 kV/cm region are the primary reason for the decrease in the transconductance. We also discuss possible solutions to this problem and examine the practicality of each solution. Shorter S/G spacing and higher doping in the source gate region are predicted to remove much of the transconductance collapse.**

***Index Terms*—GaN, HEMT, III–V nitrides, nonlinearity, transconductance collapse, velocity-field relations.**

I. Introduction

In RECENT years, significant progress has been made in GaN HEMT devices, which represent the most promising class of devices for microwave and millimeter-wave power applications. However, in III–V nitrides, the transconductance exhibits fairly large changes with the gate bias. This poses a problem for circuit design as variation of g_m, upon which many FET circuit models are predicated (see for instance [1]). It also limits large signal operation at high frequencies as well as power linearity. The gain of a transistor is critically dependent on the transconductance. Process variations during manufacture of mass production of circuits can lead to even more complicated design problems even if the variation in g_m is somehow designed around to start with.

It may be noted at this time that similar variations in the transconductance are observed in other material systems like Si, AlGaAs–GaAs, InGaAs–GaAs, etc. However, the physical reasons for those variations lie in the varying doping efficiency and miscellaneous interface effects. The structures that we consider in this paper are unintentionally doped, which means that we must look elsewhere for the cause for the collapse in g_m. The III–V nitrides exhibit some unique features (large m^*, high LO phonon energy, and large intervalley separations, etc.). It is possible that any one or more of such novel features may contribute toward this problem in GaN-based HFETs.

Manuscript received November 22, 2004; revised February 23, 2005. This work was supported by the Office of Naval Research under Grants F001681 and F004815. The review of this paper was arranged by Editor M. Anwar.

The authors are with the Department of Electrical Engineering and Computer Science, The University of Michigan, Ann Arbor, MI 48109 USA.

Digital Object Identifier 10.1109/TED.2005.848084

There are several proposed reasons for the variation in transconductance :

- interface roughness scattering [2];
- *hot* phonon scattering [3]–[5];
- nonlinear increase of source/gate (S/G) resistance with $I_{\rm DS}$ [6].

However, Monte Carlo simulations do not yield significant evidence that interface roughness scattering is the main reason for the collapse in g_m [7], especially at room temperature or higher. Further, iterative Monte Carlo calculations [8], [9] seem to suggest that hot phonon effects are not the major cause for self-heating induced variations in g_m. Recent work [6] suggests that the nonlinear increase in the S/G resistance with increase in $I_{\rm DS}$ arising from the peculiar shape of the GaN velocity-field characteristic [10] is probably the cause for this collapse in transconductance. This issue will be discussed in great detail in the sections that follow.

Most commercial simulators, such as ATLAS [1] and MEDICI, [2] are well designed for Si and GaAs. However, they are not tailored toward the unique mobility models that required in GaN. In order to explore the reasons for collapse of transconductance, we have developed our own two-dimensional (2-D) finite element method (FEM) Poisson and drift-diffusion solver combined with the mobility model obtained from our steady-state Monte Carlo simulations. In later sections, we will discuss the formalism, the transconductance results obtained from our simulation, and the physical reasons behind the collapse of g_m.

II. Formalism

In this section, we provide the basic formalism for obtaining g_m. We use the following steps.

1) Use the Monte Carlo method to obtain the velocity versus electric field (v-E) profiles; and
2) Using the v-E profiles as the input mobility model, carry out solution of 2-D Poisson and drift-diffusion equations [11] using 2-D FEM to obtain the current–voltage (I–V) curves.

A. Monte Carlo Method

We carry out steady-state Monte Carlo simulations by following the electrons motion for a time period much longer than

[1]©Silvaco

[2]©Synopsys

TABLE I
RUN PARAMETERS FOR STEADY-STATE MONTE CARLO CALCULATION

Run parameters	
Number of electrons	1
Initial energy (eV)	0.026 (300K), 0.034 (400K)
Simulation time (ns)	16
Γ (s^{-1})	7.4×10^{14}

transit time in the channel lengths studied. The process takes the following scattering mechanisms into account:

- polar optical phonon absorption and emission;
- acoustic phonon scattering;
- interface roughness scattering;
- equivalent and nonequivalent intervalley scattering;
- alloy scattering, and;
- charged dislocation scattering.

Typical parameters from literature are used [10], [12]. Since the structure considered is unintentionally doped, we ignore the ionized impurity scattering mechanism in our study [13]. The run parameters for the steady-state calculation are summarized in Table I.

B. Finite Element Solution of Poisson Equation in Two Dimensions

A Poisson equation can be written as

$$\nabla^2 E_c(x,y) = \frac{-\rho(x,y)}{\epsilon} \tag{1}$$

where E_c is the conduction band profile ρ is the total charge density and $\epsilon(z)$ is the dielectric constant in the different regions of the device. The total charge density ρ includes the doping charge, free charge from holes and electrons

$$\rho(x,y) = q\left[N_D^* - N_A^* + n_{\text{free}} - p_{\text{free}}\right] \tag{2}$$

where N_d^* and N_a^* are the effective doping concentrations, which can be expressed as

$$N_d^* = N_d \frac{1}{1 + 2e^{(E_{\text{fn}} - E_c + \Delta E_d)/k_B T}} \tag{3}$$

$$N_a^* = N_a \frac{1}{1 + 4e^{(E_v - E_{\text{fp}} + \Delta E_a)/k_B T}} \tag{4}$$

where N_d and N_a are the concentrations of donor and acceptor species and ΔE_d and ΔE_a are the corresponding impurity ionization energies. $n_{\text{free}}(z)$ and $p_{\text{free}}(z)$ are the free carrier concentrations, which can be expressed as

$$n_{\text{free}} = N_c F_{1/2}\left(\frac{E_{\text{f}} - E_c}{k_B T}\right)$$

$$p_{\text{free}} = N_v F_{1/2}\left(\frac{E_v - E_{\text{f}}}{k_B T}\right)$$

where N_c and N_v are the effective density of states and $F_{1/2}$ is the half-order Fermi integral. $E_v(z)$ is the valence band energy. After solving the Poisson equation, we need to solve the drift-diffusion equations

$$\mathbf{J_n} = -\mu_n n \boldsymbol{\nabla} E_c + q D_n \boldsymbol{\nabla} n, \tag{5}$$

$$\mathbf{J_p} = \mu_p p \boldsymbol{\nabla} E_v - q D_p \boldsymbol{\nabla} p \tag{6}$$

where $\mu_{n,p}$ are the mobilities of the electrons and holes obtained by Monte Carlo method, and $D_{n,p}$ are the diffusion coefficients of electrons and holes. n and p above should be implicitly understood to be functions of x and y. Using the Einstein relation [14], $D/\mu = k_B T/q$, (5) and (6) can be rewritten as (dropping the vector notation)

$$J_n = -\mu_n n \nabla E_{\text{fn}}, \tag{7}$$

$$J_p = \mu_p p \nabla E_{\text{fp}} \tag{8}$$

where E_{fn} and E_{fp} are quasi-fermi levels of electrons and holes, respectively. Using the continuity equation

$$\nabla J_n = qR, \tag{9}$$

$$\nabla J_p = -qR \tag{10}$$

where R is the Shockley-Read-Hall [14], [15] recombination/generation rate, shown in (11) at the bottom of the page, where $\tau_{n,p}$ are electron and hole lifetimes and E_t is the trap energy. It is well known that there is a large polarization charge at the AlGaN-GaN interface [16]. For the charge control model, the semiconductor interface is treated as an abrupt heterojunction between channel and barrier materials. The following boundary condition for the heterojunction interface accounts for the polar charges at the interface:

$$\epsilon_1 \mathbf{E_1} + \mathbf{P_1} = \epsilon_2 \mathbf{E_2} \tag{12}$$

where $\epsilon_{1,2}$ are the dielectric constants and $\mathbf{E_{1,2}}$ are the electric fields at the interface. $\mathbf{P_1}$ is the polarization at the interface [17]. Equation (1) also needs to satisfy another boundary condition at the interface

$$E_{c1} + \triangle E_c = E_{c2} \tag{13}$$

where E_c is conduction band energy profile which can be expressed as $\nabla \mathbf{E}$. $\triangle E_c$ is conduction band discontinuity at the abrupt heterojunction interface. At the drain and source ends, Ohmic contact is assumed to exist and at the gate contact, Schottky contact is assumed, which leads to

$$E_c = V_G + \Phi_B$$

where Φ_B is the Schottky barrier height. To solve the drift diffusion equations [(5) and (6)], Slotboom variables [18] and Gümmel [19] iteration method are used for their linear properties for drift-diffusion equations and global convergence. LAPACK 3 is used the solve the matrix generated by 2-D FEM.

$$R = \frac{pn - n_i^2}{\tau_{n_0}\left(p + n_i \exp\left(\frac{E_i - E_t}{K_B T}\right)\right) + \tau_{p_0}\left(n + n_i \exp\left(\frac{E_t - E_i}{K_B T}\right)\right)} \tag{11}$$

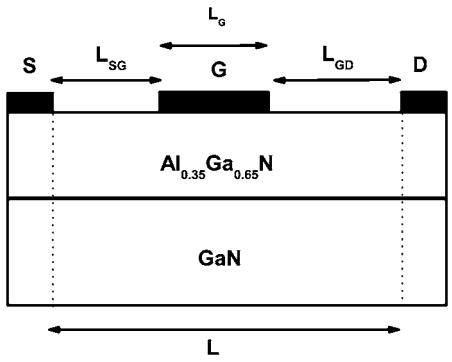

Fig. 1. $Al_{0.35}Ga_{0.65}N$–GaN HFET structure. The source/drain spacing, L, is taken to be 1.9 μm. $L_{\rm SG}$ and $L_{\rm GD}$ are the S/G and the source/drain distances, respectively.

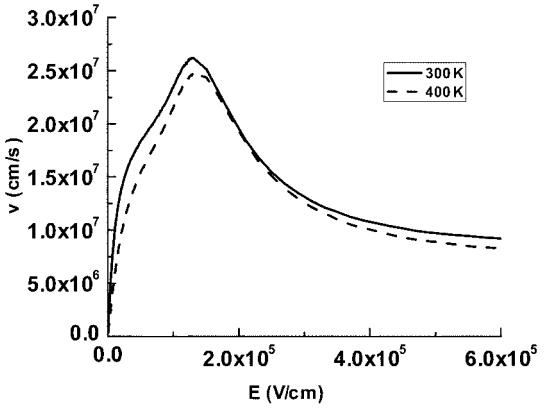

Fig. 2. Steady-state velocity field relations for 300 K and 400 K.

III. Results

We consider a heterojunction field-effect transistor structure ($Al_{0.35}Ga_{0.65}N$–GaN) shown in Fig. 1. The polarization sheet charge density at the heterointerface is assumed to be 1.6×10^{13} cm^{-2}. Unless otherwise stated, the source/drain spacing, L, is taken to be 1.9 μm. It may be noted at this point that since the structure is not self-aligned, the channel length and the gate length are not identical as in self-aligned structures ($L_G \neq L$).

Fig. 2 shows the steady-state velocity-field (v-E) profile obtained from steady-state Monte Carlo simulation. We find that the peak velocity for this profile appears at $E \sim 1.25 \times 10^5$ V/cm. It is important to note that there is a *hump* in the velocity-field characteristic, localized between $E = 5 \times 10^3$ V/cm and $E = 4 \times 10^4$ V/cm. This hump occurs at a field that turns out to be quite important in the S/G region under normal biasing conditions. As mentioned in Section II, we used the v-E profiles as our mobility model. Our model can also be used to calculate the current-voltage (I–V) characteristics. Fig. 3 shows a few I–V curves obtained from our 2-D FEM Poisson and drift-diffusion solver for $L_G = 0.25$ μm. As can be seen, the I–V curves show a clear saturation region, and are in fair agreement with experimental results.

In Fig. 4, we show g_m and $I_{\rm DS}$ as a function of gate bias. For this structure with $L_G = 0.25$ μm, we choose $L_{\rm SG} = 0.65$ μm. In results shown later, other configurations are also

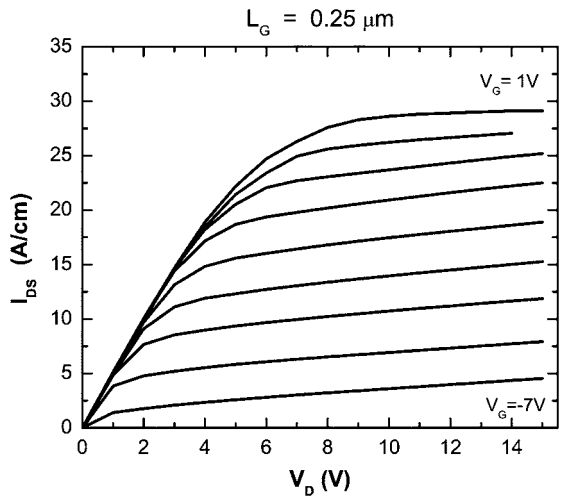

Fig. 3. I–V relations for $L_G = 0.25$ μm.

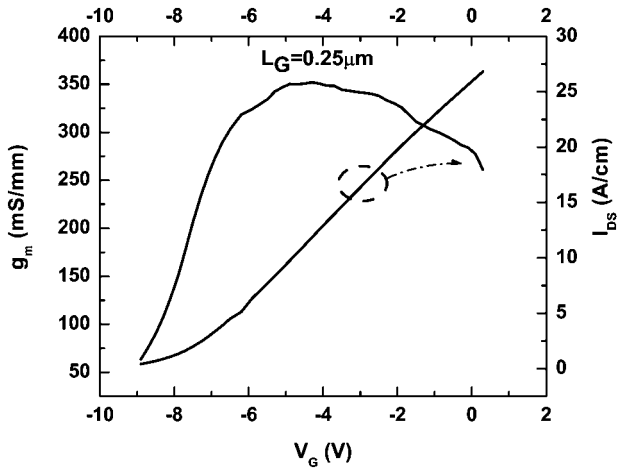

Fig. 4. Variation of g_m and $I_{\rm DS}$ with gate bias for $L_G = 0.25$ μm. $L_{\rm SG} = 0.65$ μm.

considered. The drain bias, $V_{\rm DS}$ is fixed at 10 V for all the results that follow. As can be seen from Fig. 4, the collapse in the transconductance is rather marked. This behavior is very similar to the observed experimental results [6]. The calculated values are slightly higher than the experimental results as the actual mobilities in the channel may be somewhat lower than the ones predicted by the Monte Carlo calculation. This can happen due to self-heating in the channel under continuous operation [20]. The physical reasons for this collapse are not obvious, per se. In the results that follow, we attempt to elucidate the reasons for this behavior. The current carried by a set of moving electrons can be written as

$$I = nev$$

where n is the carrier density and v is the carrier velocity. Transconductance can thus be expressed as

$$g_m = \frac{\Delta I}{\Delta V_G} = \underbrace{\left(\frac{\Delta n}{\Delta V_G}\right) ev}_{I} + \underbrace{\left(\frac{\Delta v}{\Delta V_G}\right) ne}_{II}. \quad (14)$$

TABLE II
GATE-LENGTH AVERAGED ENSEMBLE AVERAGED ELECTRON VELOCITIES FOR $L_G = 0.25\ \mu$m. THE INTERFACE ROUGHNESS SCATTERING IS CONSIDERED IN THE SIMULATION. THERE IS A VERY WEAK DEPENDENCE ON THE GATE BIAS

V_G (V)	v_{avg} (10^7 cm$\cdot$ s^{-1})
-2	2.34
-3	2.30
-4	2.23

Numerical simulations and capacitance-voltage measurements suggest that the change in the number of electrons is $\propto \Delta V_G$. If we consider the two terms in (14), the only possible remaining source of change in g_m is the modulation of the carrier velocity, Δv (term II). If Δv were proportional to ΔV_G or zero, it would imply a transconductance that is constant as a function of V_G. However, that is clearly not the case, either numerically (Fig. 4) or experimentally [21]. It must be noted at this point that this variation in g_m does not refer to the precipitous decline in the transconductance for $V_G < -6$ V, as the physical reasons for that decrease lie in the depletion of the channel at those gate biases. Ensemble Monte Carlo simulations under the gate region show that the gate-length averaged ensemble averaged electron velocities (Table II) do not change much with the change in gate bias. Thus

$$\frac{\Delta v}{\Delta V_G} \sim 0.$$

This is due to that the electric field in the gate region (Fig. 5) corresponds almost to the velocity saturation region in the velocity field characteristic ($E > 2 \times 10^5$ V/cm—see Fig. 2). The effect of interface scattering is very weak because the interface roughness scattering rate decreases dramatically in the high field region [7] so that polar optical phonon absorption and emission and acoustic phonon scattering dominate the electron transport in the gate region. This means that any increase in the electric field only impacts the carrier density in the gate region, not the carrier velocities. However, the structure depicted in Fig. 1 is not self-aligned (as indeed are most GaN HFETs). A considerable fraction of the conductive channel lies outside the gate region (a total length of $L_{\rm SG} + L_{\rm GD}$). This is often much greater than the gate length itself, especially for shorter gate devices. Thus, the carrier velocity outside the channel is an important factor than needs to be taken into account when determining device performance. Our simulation indicates that electric field in source gate region changes as the V_G changes as shown in Fig. 5. The total variation in the electric field is from 5×10^3 V/cm to 2×10^4 V/cm when the gate bias is changed from -4 V to 0 V. This corresponds to the low-field nonlinear region in the v-E characteristics (the *hump* referred to earlier). This implies an extra, bias-dependent, contribution to the source gate resistance. This, as will be seen later, is a major source of the decrease in the transconductance.

The physical reason for this nonlinearity in the low field region can be seen from Fig. 6. We know that the GaN has a relatively high effective mass ($\sim 0.2\ \mathrm{m}_o$) and high LO phonon energy (~ 0.09 eV). Therefore, the peak velocity appears

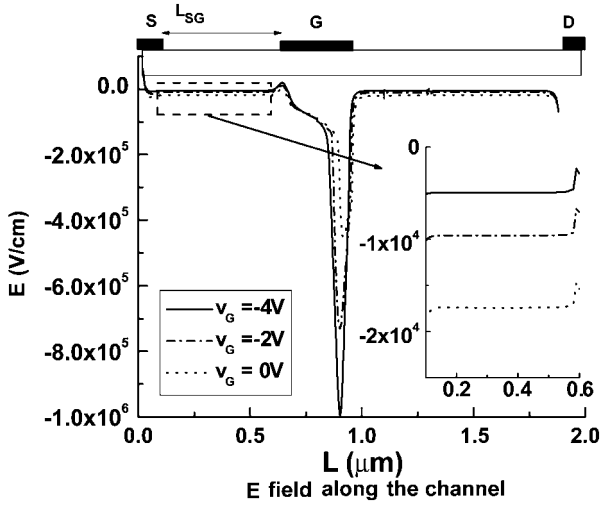

Fig. 5. Electric field along the channel at AlGaN-GaN interface for the UID case shown in Fig. 4.

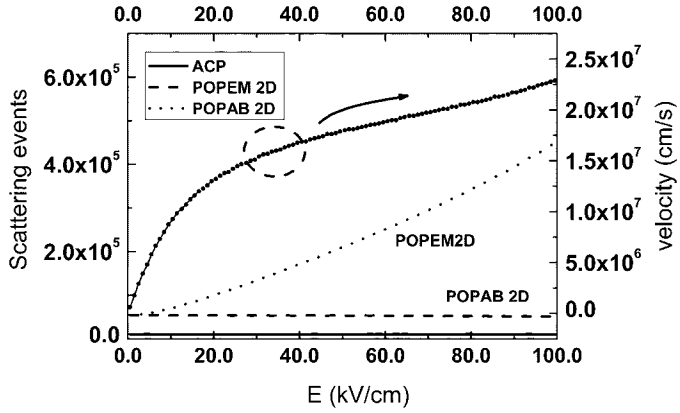

Fig. 6. Number of scattering events corresponding to the 2-D polar optical emission (POPEM2D) and 2-D polar optical absorption (POPAB2D) processes as a function of the electric field. The marked curve is a portion of the velocity-field characteristic.

near 1.25×10^5 V/cm, which is 40 times larger than the corresponding electric field in GaAs. In the very low field region, steady-state Monte Carlo simulation shows that the average electron energy is lower than LO phonon energy, which implies a low probability for the 2-D variant of the polar optical phonon emission process (POPEM2D) [22], [23]. As the electric field increases, the probability of an electron acquiring enough energy to surmount the LO phonon energy is increased. Therefore, the gradual increase in the strength of the POPEM2D process slows down the rate of increase of electron velocity and results in the *hump*. In other materials such as GaAs and InAs, this nonlinearity does occur but at much lower energies as the LO phonon energy is much lower for those systems. Further, the peak in the v-E characteristic for those systems occur at a much lower field and the carriers are already in the saturation region for the usual fields during transport. Thus the field outside the gate region for the same structure implemented in III–V arsenide technology would exhibit $\Delta v \sim 0$, and hence little or no variation in the transconductance.

In order to verify if the *hump* in the low-field region is the reason for the collapse in the transconductance, we carried out

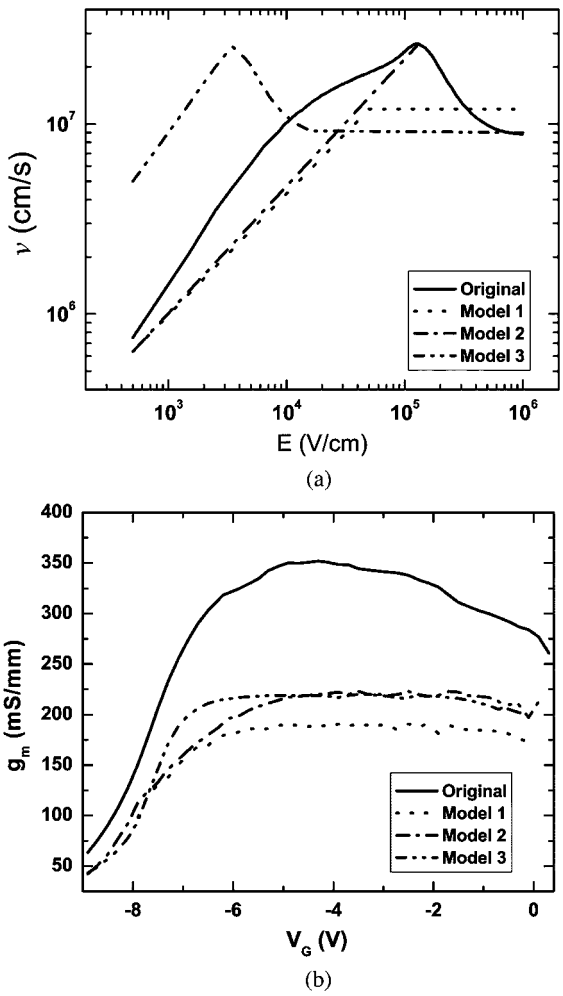

Fig. 7. (a) Actual and three-test mobility models in the low-field region. (b) Corresponding bias dependence of transconductance.

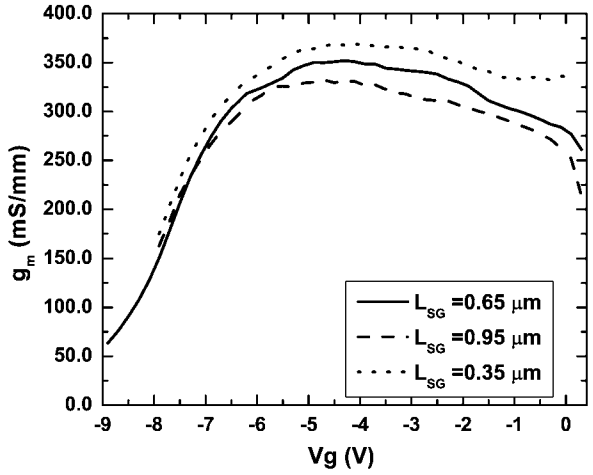

Fig. 8. Bias dependence of g_m for different source gate spacings. The channel is assumed to be unintentionally doped.

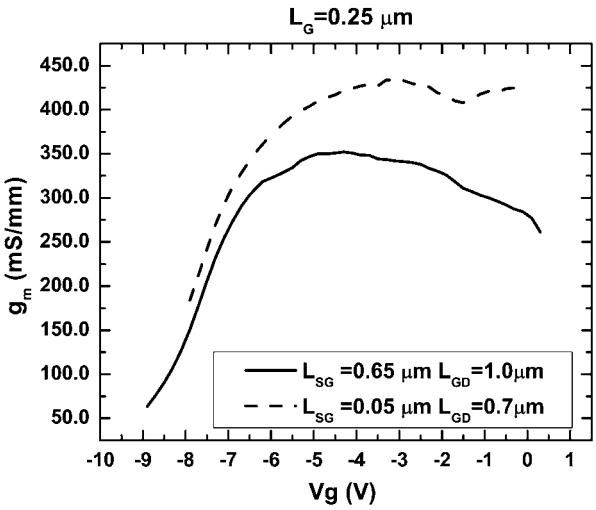

Fig. 9. Bias dependence of g_m for more self-aligned structures. The channel is assumed to be unintentionally doped.

calculations for many different mobility models depicted in Fig. 7. The solid line in Fig. 7 corresponds to the actual mobility model in the HFET (Fig. 2). We consider three different test mobility models. In test model 1, we use a monotonic relation for v-E and then impose a saturation in the velocity. In test mobility model 2, the velocity increases linearly and the behavior at high fields is taken to be the same as it is for GaN. In test model 3, we assume a much faster increase in the velocity, corresponding to a much lower effective mass (for materials like GaAs, InN, InAs, etc.). In all three cases, we observe a transconductance that is much more insensitive to change in gate bias in the region of interest. Thus, we can conclude that the source of the collapse in the transconductance observed for the actual mobility model is a result of the nonlinearity in the low-field v-E characteristic.

Since the nonlinear variation of the source gate resistance $(R_{\rm SG})$ (and to a lesser extent, gate drain resistance, $R_{\rm GD}$, due to the shape of the electric field profile) is an important factor affecting transconductance, it is logical to investigate the effect of reducing the magnitude of the resistance as a possible solution for improving the bias dependence of g_m. We investigate two possible approaches to achieve that goal :

1) *Making the structure more self-aligned* In Fig. 8, we model the effect of reducing the source gate spacing. We find that decreasing the spacing between the source and the gate is effective in preventing the collapse in transconductance. In this case, the total source drain spacing, L, is not changed. Let us consider a more radical change in the structure of the device. In Fig. 9, we model the effect of reducing the source gate and gate drain spacings, in two different cases. Not only is the total magnitude of the transconductance enhanced significantly by reducing $L_{\rm SG}$ and $L_{\rm GD}$, but also the absolute and relative maximal variations in the transconductance as a function of the gate bias, suppressed. To estimate the effect of this, we summarize the results in the first two entries in Table III. The relative variation in g_m is thus reduced about four times by using a more self-aligned structure.
2) *Increasing the doping in the S/G region* In Fig. 10, we model the effects of heavy doping in the source gate

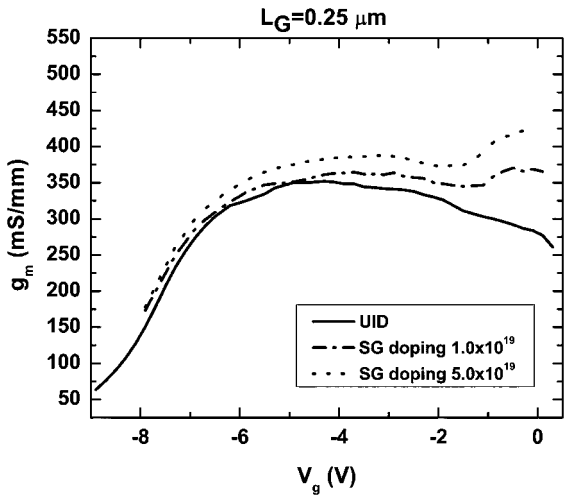

Fig. 10. Effect of doping on the bias dependence of g_m. The doping is assumed to be introduced only in the SG region. The dopants are assumed to be fully ionized.

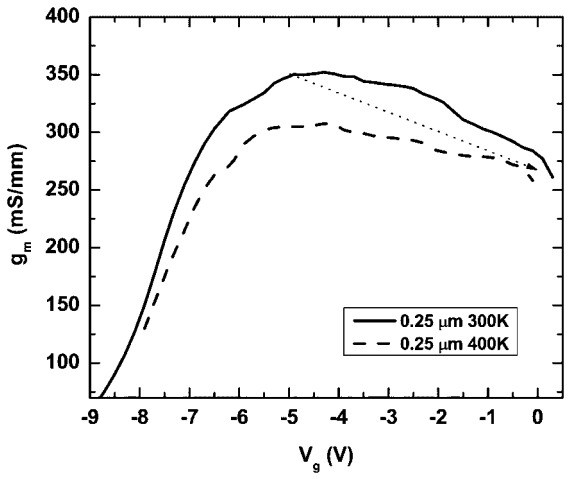

Fig. 11. Bias dependence of g_m for two different temperatures. The dotted arrow line shows the possible trend of the g_m as the temperature increases with higher drain current.

TABLE III
EFFECTIVENESS OF USING A MORE SELF-ALIGNED STRUCTURE AND DOPED SOURCE-GATE REGIONS. STRUCTURE I : THE USUAL NON-SELF-ALIGNED STRUCTURE CONSIDERED IN MOST OF OUR RESULTS. STRUCTURE II : A MORE SELF-ALIGNED STRUCTURE WITH $L_{\rm SG} = 0.05$ μm AND $L_{\rm GD} = 0.7$ μm. STRUCTURE III : THE USUAL NON-SELF-ALIGNED STRUCTURE, BUT WITH SG REGION DOPED AT 1×10^{19} cm^{-3}. STRUCTURE IV : SAME AS STRUCTURE III, BUT WITH DOPING DENSITY $= 5 \times 10^{19}$ cm^{-3}. PEAK gm IS TAKEN TO BE THE VALUE OF TRANSCONDUCTANCE JUST BEFORE THE COLLAPSE

Structure	Peak g_m (mS/mm)	Δg_m (mS/mm)	Relative, $\Delta g_m/g_m$ (dimensionless)
I	~ 340	~ 60	17.7%
II	~ 430	~ 20	4.7%
III	~ 360	~ 15	4.2%
IV	~ 390	~ 45	11.5%

region near the AlGaN-GaN interface. We assume that the dopants are fully ionized. The effect of increasing the doping in the SG region is to reduce the resistivity and hence $R_{\rm SG}$. This decreases the magnitude of the field-dependent change in $R_{\rm SG}$ due to nonlinearities in the v-E characteristic. The results of this approach are summarized in the last two entries of Table III.

As mentioned earlier, the interface roughness scattering is not dominant in the high-fieldgate region. For the channel outside the gate region, the interface roughness scattering is stronger due to the low electric field outside the gate. However, the channel charge density outside the gate region is a weak function of the gate voltage. Thus, interface roughness scattering rate is almost constant, and does not contribute to the degradation of g_m.

Let us now consider the effect of self-heating for continuous operation. As shown in Fig. 2, the low-field mobility for $T = 400$ K ($T = 400$ K is chosen merely as an illustrative case) is lower than it is at $T = 300$ K. We present the calculations of g_m at these two temperatures in Fig. 11. At higher current levels for higher gate biases, the resultant self-heating of the device is likely to act as a self-limiting mechanism due to enhanced scattering (as the mobility model at 400 K suggests). Thus, the drain current, and consequently, the transconductance, are likely to deviate even more from their predicted values at 300 K due to local self-heating effects at higher gate biases (the dotted arrow line in Fig. 2). Proper accounting of the effect of self-heating would require application of energy balance equations and far more complicated Monte Carlo treatment than used in this work. This effect is likely to be important when designing high-power amplifiers and requires further study.

IV. CONCLUSION

In this paper, we have used three different test mobility models to prove that nonlinearity in the low-field v-E characteristic is primarily responsible for the observed collapse of transconductance in III–V nitrides. This leads to a nonlinearity in the S/G resistance, $R_{\rm SG}$. Reducing the gate source distance to reduce the effects of nonlinearity is a feasible method to improve the transconductance behavior. Use of heavy doping in the S/G region, which reduces the magnitude of the resistance, is another possible way of reducing the magnitude of $R_{\rm SG}$. Therefore, changing from nonself-aligned structures to more self-aligned structures, or enhancing the doping in the source gate region, could constitute a solution to the transconductance problem. Although it does appear that the low-field nonlinearity is a very important and fundamental reason for the collapse in the transconductance, other reasons such as self-heating may also contribute in case of continuous operation. Other methods, such as use of a double channel structure [21], have also been proposed which show promising results. Designing a composite channel to reduce the nonlinearity in the low electric field region [10] is another possible method.

ACKNOWLEDGMENT

The authors would like to thank T. Palacios at UCSB for his help in calibrating the Poisson FEM solver with ATLAS.

REFERENCES

[1] P. R. Gray and R. G. Meyer, *Analysis and Design of Analog Integrated Circuits*. New York: Wiley, 1993.

[2] J. R. Juang, T.-Y. Huang, T.-M. Chen, M.-G. Lin, G.-H. Kim, Y. Lee, C.-T. Liang, D. R. Hang, Y. F. Chen, and J.-I. Chyi, "Transport in a gated $Al_{0.18}Ga_{0.82}N$-GaN electron system," *J. Appl. Phys.*, vol. 94, no. 5, pp. 3181–3184, 2003.
[3] A. Matulionis, J. Liberis, L. Ardaravicius, J. Smart, D. Pavlidis, S. Hubbard, and L. F. Eastman, "Hot-phonon limited electron energy relaxation in AlN–GaN," *Int. J. High Speed Electron. Syst.*, no. 2, pp. 2002–2002, 2002.
[4] L. Ardaravicius, A. Matulionis, J. Liberis, O. Kiprijanovic, M. Ramonas, L. F. Eastman, J. R. Shealy, and A. Vertiatchikh, "Electron drift velocity in AlGaN/GaN channel at high electric fields," *Appl. Phys. Lett.*, vol. 83, no. 19, pp. 4038–4040, 2003.
[5] A. Matulionis, J. Liberis, L. Ardaravicius, L. F. Eastman, J. R. Shealy, and A. Vertiatchikh, "Hot-phonon lifetime in AlGaN/GaN at a high lattice temperature," *Semicond. Sci. Technol.*, vol. 19, no. 4, pp. S421–S423, 2004.
[6] T. Palacios, S. Rajan, L. S. amd, A. Chakraborty, S. Heikman, S. Keller, S. P. DenBaars, and U. K. Mishra, "Influence of the access resistance in the RF performance of mm-wave AlGaN–GaN HEMTs," in *Proc. 62nd Device Research Conf.*, Jun. 2004, pp. 75–76.
[7] T. Li, R. P. Joshi, and C. Fazi, "Monte Carlo evaluations of degeneracy and interface roughness effects on electron transport in AlGaN-GaN heterostructures," *J. Appl. Phys.*, vol. 88, no. 2, pp. 829–837, 2000.
[8] J. M. Barker, D. K. Ferry, S. M. Goodnick, D. D. Koleske, A. Allerman, and R. J. Shul, "High field transport in GaN/AlGaN heterostructures," *J. Vac. Sci. Technol. B, Microelectron. Process. Phenom.*, vol. 22, no. 4, pp. 2045–2050, 2004.
[9] M. Singh, Y.-R. Wu, and J. Singh, "Velocity overshoot effects and scaling issues in III–V nitrides," *IEEE Trans. Electron Devices*, vol. 52, no. 3, pp. 311–319, Mar. 2005.
[10] M. Singh and J. Singh, "Design of high electron mobility devices with composite nitride channels," *J. Appl. Phys.*, vol. 94, no. 4, pp. 2498–2506, Aug. 2003.
[11] Y.-R. Wu, M. Singh, and J. Singh, "Gate leakage suppression and contact engineering in nitride heterostructures," *J. Appl. Phys.*, vol. 94, no. 9, pp. 5826–5831, 2003.
[12] I. Vurgaftman, J. R. Meyer, and L. R. Ram-Mohan, "Band parameters for III–V compound semiconductors and their alloys," *J. Appl. Phys.*, vol. 89, no. 11, pp. 5815–5875, 2001.
[13] R. F. Davis, A. M. Roskowski, E. A. Preble, J. S. Speck, B. Heying, J. A. Freitas Jr, E. R. Glaser, and W. E. Carlos, "Gallium nitride materials—Progress, status, and potential roadblocks," *Proc. IEEE*, vol. 90, no. 6, pp. 993–1005, Jun. 2002.
[14] J. Singh, *Physics of Semiconductors and Their Heterostructures*. New York: McGraw-Hill, 1993.
[15] S. M. Sze, *Semiconductor Devices Physics and Technology*. New York: Wiley, 1985.
[16] O. Ambacher, J. Smart, J. R. Shealy, N. G. Weimann, K. Chu, M. Murphy, W. J. Schaff, L. F. Eastman, R. Dimitrov, L. Wittmer, M. Stutzmann, W. Rieger, and J. Hilsenbeck, "Two-dimensional electron gases induced by spontaneous and piezoelectric polarization charges in N-and Ga-face AlGaN–GaN heterostructures," *J. Appl. Phys.*, vol. 85, pp. 3222–3233, 1999.
[17] O. Ambacher, J. Majewski, C. Miskys, A. Link, M. Hermann, M. Eickhoff, M. Stutzmann, F. Bernardini, V. F. V. Tilak, B. Schaff, and L. F. Eastman, "Pyroelectric properties of Al(In)GaN–GaN hetero-and quantum well structures," *J. Phys. Condens. Matt.*, vol. 14, no. 13, pp. 3399–3434, 2002.
[18] J. W. Slotboom, "Computer-aided two-dimensional analysis of bipolar transistors," *IEEE Trans. Electron Devices*, vol. ED-20, no. 6, pp. 669–679, Jun 1973.
[19] H. K. Gummel, "A self-consistent iterative scheme for one-dimensional steady-state transistor calculations," *IEEE Trans. Electron Devices*, vol. ED-11, no. 5, pp. 455–465, May 1964.
[20] A. Chini, R. Coffie, G. Menghesso, E. Zanoni, D. Buttari, S. Heikman, S. Keller, and U. K. Mishra, "2.1 A/mm current density AlGaN/GaN HEMT," *Electron. Lett.*, vol. 39, no. 7, pp. 625–626, 2003.
[21] T. Palacios, A. Chini, D. Buttari, S. Heikman, S. Keller, S. P. DenBaars, and U. K. Mishra, "Use of multichannel heterostrucures to improve the access resistance and f_T linearilty in gan-based HEMTs," in *Proc. 62nd Device Research Conf.*, 2004, pp. 41–42.
[22] K. Yokoyama and K. Hess, "Monte Carlo study of electronic transport in $Al_{1-x}Ga_xAs/GaAs$ single-well heterostructures," *Phys. Rev. B, Condens. Matter*, vol. 33, no. 8, pp. 5595–5606, 1986.
[23] Y. Zhang and J. Singh, "Monte Carlo studies of two dimensional transport in GaN/AlGaN transistors : Comparison with transport in AlGaAs–GaAs channels," *J. Appl. Phys.*, vol. 89, no. 1, pp. 386–389, 2001.

Yuh-Renn Wu (S'03) received the B.S. degree in physics and the M.S. degree in communication engineering from National Taiwan University, Taipei, Taiwan, R.O.C., in 1998 and 2000, respectively. He is currently pursuing the Ph.D. degree in electrical engineering at the Department of Electrical Engineering and Computer Science, University of Michigan, Ann Arbor.

His current research includes theoretical studies of vertical and parallel transport in III-V nitride heterostructures, ferroelectrics, and opto-electronic devices.

Madhusudan Singh (S'99) received the M.Sc. (Integrated) degree in physics from the Indian Institute of Technology, Kanpur, India, in 1999. He received the M.S. degrees in electrical engineering and mathematics from The University of Michigan, Ann Arbor, in 2003, where he is currently pursuing the Ph.D. degree in electrical engineering at the Department of Electrical Engineering and Computer Science.

His current research includes theoretical studies of vertical and parallel transport in III-V nitride heterostructures, ferroelectrics, and organic semiconductors.

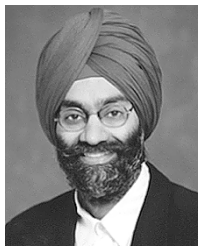

Jasprit Singh received the Ph.D. degree in solid-state physics from the University of Chicago, Chicago, IL, in 1980, where he worked in the area of disordered semiconductors.

He then spent three years at the University of Southern California, Los Angeles, two years at Wright-Patterson AFB, Ohio, and has been at The University of Michigan, Ann Arbor, since 1985. His area of research is physics and design of semiconductor heterostructure devices. He has worked on electronic and opto-electronic devices based on traditional III-V materials, HgCdTe, SiGe, and the nitrides. His current research is exploiting ferroelectric materials within conventional semiconductor devices. His recent books are *Modern Physics for Engineers*, (New York: Wiley Interscience, 1999) and *Semiconductor Devices: Basic Principles*, (New York: Wiley, 2001).